1 Atmospheric new particle formation characteristics in the Arctic as 2 measured at Mount Zeppelin, Svalbard, from 2016 to 2018

3 Haebum Lee[1], KwangYul Lee[1], Chris Rene Lunder[2], Radovan Krejci[3], Wenche Aas[2], Jiyeon Park[4], Ki-
4 Tae Park[4], Bang Yong Lee[4], Young-Jun Yoon[4,*], and Kihong Park[1,*]

5 [1]School of Earth Sciences and Environmental Engineering, Gwangju Institute of Science and Technology, 123
6 Cheomdangwagiro, Buk-gu, Gwangju 61005, Republic of Korea.
7 [2]Department for Atmospheric and Climate Research, NILU - Norwegian Institute for Air Research, Kjeller, Norway.
8 [3]Department of Environmental Sciences and the Bolin Centre for Climate Research, Stockholm University, Stockholm, SE-
9 106 91, Sweden.
10 [4]Korea Polar Research Institute, 26, Songdo Mirae-ro, Yeonsu-Gu, Incheon, Korea.

12 *Correspondence to: Kihong Park (kpark@gist.ac.kr) and Young-Jun Yoon (yjyoon@kopri.re.kr)

13 **Abstract.** We conducted continuous measurement of nanoparticles down to 3 nm size in the Arctic at Mount Zeppelin, Ny

14 Ålesund, Svalbard, from 2016 to 2018, providing a size distribution of nanoparticles (3–60 nm) with a higher resolution than

15 ever before. A significant number of nanoparticles as small as 3 nm were often observed during new particle formation (NPF),

16 particularly in summer, suggesting that these were likely produced near the site rather than being transported from other regions

17 after growth. The average NPF frequency per year was 24% having the highest percentage in August (63%). The average

18 particle formation rate (J) for 3–7 nm particles was 0.1 cm^{-3} s^{-1} and the average growth rate (GR) was 2.62 nm h^{-1}. Although

19 NPF frequency in the Arctic was comparable to that in continental areas, the J and GR were much lower. The number of

20 nanoparticles increased more frequently when air mass originated over the south and southwest ocean regions; this pattern

21 overlapped with regions having strong chlorophyll-α concentration and dimethyl sulfide (DMS) production capacity

22 (southwest ocean), and was also correlated with increased daily NH_3 concentration, suggesting that marine biogenic and animal

23 sources were responsible for gaseous precursors to NPF. Our results show that previously developed NPF occurrence criteria

24 (low loss rate and high cluster growth rate favor NPF) are also applicable to NPF in the Arctic.

25 1 Introduction

26   The Arctic climate system is affected by the region's snow-covered land, sea ice, and ocean, making the region

27 vulnerable to global climate change (Jeffries and Richter-Menge, 2011). Greenhouse gases and aerosols are significant factors

28 affecting the regional climate (Quinn et al., 2007; IPCC, 2014). In particular, aerosols in the ambient atmosphere affect the

29 radiation balance by scattering or absorbing incoming solar light (direct effect) (Toon and Pollack, 1980; Satheesh et al., 2005)

30 and forming clouds by acting as cloud condensation nuclei (CCN) (indirect effect) (Merikanto et al., 2009).

31   New particle formation (NPF), which significantly enhances the number of particles in the ambient atmosphere, has

32 been observed in various locations and at various times (Kulmala et al., 2004; Wang et al., 2017; Yu et al., 2017). In favourable

33 conditions, newly formed nanoparticles can, through condensation and coagulation, grow to sizes allowing the formation of

34 CCN. NPF is observed regardless of pollution level, from very clean (e.g., background sites) to heavily polluted (e.g., urban

35 sites), suggesting that various pathways are involved depending on the location and time (Kulmala et al., 2004; Wang et al.,

36 2017). Nucleation can occur almost anytime in diverse environments, but NPF is observed only when freshly nucleated clusters

37 grow to a detectable size (1–3 nm) (McMurry et al., 2010). Previously developed criteria for NPF occurrence suggest that a

38 low loss (or scavenging) rate and high growth rate (GR) of clusters increase fresh nuclei survivor probability and thus favoring

39 NPF, while a high loss rate and low cluster GR suppress it (Kuang et al., 2012).

40   In the Arctic, specific phenomenon called "Arctic haze" related to long range transport of polluted air masses

41 typically occurs in the late winter and early spring (Iziomon et al., 2006; O'Neill et al., 2008, Hirdman et al., 2010). The Arctic

42 haze is associated with elevated concentrations of accumulation-mode particles. (Radke et al., 1984; Shaw, 1995; Law and

43 Stohl, 2007; Quinn et al., 2007). High concentration of accumulation-mode particles results in a high condensational sink (CS)

44 for precursor vapors, which could suppress NPF. The NPF in the Arctic was often reported in summer, when the CS was

45 smaller (Wiedensohler et al., 1996; Covert et al., 1996; Sharma et al., 2013; Willis et al., 2016; Croft et al., 2016). In addition,

46 strong biogenic production from marine and coastal environments in the Arctic region (e.g., Alaska, Alert, and Svalbard) was

47 reported to be linked to NPF due to an increased amount of biogenic sulfur compounds such as dimethyl sulfide and its

48 oxidative products (methane sulfonate and biogenic sulfate) (Leaitch et al., 2013; Park et al., 2017). Like in sulfuric acid-rich

49 regions, organic-based new particles were observed in pristine environments (Quinn et al., 2002; Leaitch et al., 2013;

50 Heintzenberg et al., 2015). Asmi et al. (2016) reported that NPF was more common in air masses of oceanic origin compared

51 to continental ones in the Arctic (Tiksi station, Russia). Dall'Osto et al. (2018) suggested that NPF at Station Nord in North

52 Greenland was related to seasonal sea-ice cycles (i.e., the NPF was associated with air masses coming from open water and

53 melting sea-ice regions).

54   There are several past studies of NPF at the Zeppelin Observatory at Mount Zeppelin in Svalbard, Norway (Tunved

55 et al., 2013; Dall'Osto et al., 2017; Heintzenberg et al., 2017). The location of the station is 474 m above sea level and ~2 km

56 from a small scientific community, with minimal effects from anthropogenic sources; its unique geographical location is ideal

57 for investigating NPF in the Arctic environment. Tunved et al. (2013) studied seasonal variations in particle size distribution

58 and NPF based on aerosol size distribution data (10–790 nm) from 2000 to 2010. Heintzenberg et al. (2017) developed a new

59 NPF search algorithm using size distribution data (5–630 nm) from 2006 to 2015. Dall'Osto et al. (2017) determined the

60 relationship between NPF and the extent of Arctic sea-ice melt using size distribution data (10–500 nm) from 2000 to 2010

61 and used hourly data to classify the size distributions and NPF types. It was reported that NPF at the Mount Zeppelin site

62 mostly occur during summer, which was attributed to the low CS and high biological activity in summer (Leaitch et al., 2013;

63 Heintzenberg et al., 2015; Park et al., 2017). NPF occurrence was low during the Arctic haze (with high CS) period (Covert et

64 al., 1996; Tunved et al., 2013; Croft et al., 2016). Heintzenberg et al. (2017) suggested that NPF at the Mount Zeppelin site

65 was related to solar flux and sea surface temperature, affecting marine biological processes and photochemical reactions with

66 less CS. They reported the potential source regions for NPF to be the marginal-ice and open-water areas between northeastern

67 Greenland and eastern Svalbard. Although particle size distribution data from the Mount Zeppelin site are available (Ström et

68 al., 2003; Tunved et al., 2013; Dall'Osto et al., 2017), no data regarding the size distribution of nanoparticles smaller than 5

69 nm are available, though these could provide greater insight into NPF characteristics. Currently, the initial formation and

70 growth of nanoparticles below 10 nm cannot be resolved, and weak NPF events with no substantial particle growth up to 10

71 nm cannot be detected.

72   In this study, we measured size distribution of nanoparticles down to 3 nm for the first time at Zeppelin station. and

73 obtained continuous size distributions of 3–60 nm particles every 3 min from 2016 to 2018. This allowed the size distribution

74 of nanoparticles to be determined with a higher resolution than ever before, enabling better identification of whether freshly

75 nucleated particles formed on-site or were transported from other regions after substantial growth. We were also able to detect

76 NPF events when particle growth was terminated below 10 nm. The particle size distributions were classified into several

77 clusters, and the seasonal (monthly), daily, and diurnal variations of the nanoparticle concentrations were examined. We also

78 applied the NPF criteria to Arctic data to determine whether or not NPF should occur [10] and investigated the characteristics of

79 NPF events related to formation rate, GR, CS, and meteorological parameters. Finally, potential source regions for NPF were

80 explored using air mass backward trajectory and satellite-derived chlorophyll-α concentration data.

81

2 Methods

83   The measurement site was located at the Zeppelin Observatory at Mount Zeppelin, Svalbard (78°54'N, 11°53'E),

84 which is 474 m above sea level and ~2 km from the small scientific community in Ny-Ålesund, Norway (78°55'N, 11°56'E)

85 (Figure 1). Ny-Ålesund lies within the west Spitsbergen current at the northernmost point of the warm Atlantic influx; this

86 location provides an ideal location for observing climate parameters and investigating the long-range transport route by which

87 contamination is often carried via southerly air masses (Neuber et al., 2011). The dominant wind patterns (east and southeast

88 from the Kongsvegen glacier (40%) and northwest from the Kongsfjorden channels (14%) during the measurement period)

89 and elevation suggest that the effects of local sources on the Zeppelin Observatory are small (Beine et al., 2001).

90   An air inlet with a flow rate of 100 L min^{-1} was used to introduce ambient aerosols into the instruments. The flow

91 temperature was maintained above 0 ℃ to prevent ice and frost formation in the tube. The observatory was kept warm and

92 dry, with an indoor temperature and relative humidity (RH) of ~20 ℃ and < 30%, respectively (Tunved et al., 2013;

93 Heintzenberg et al., 2017). A nano-scanning mobility particle sizer consisting of a nano-differential mobility analyzer (nano-

94 DMA) (model 3085, TSI, USA) and an ultrafine condensation particle counter (model 3776, TSI, USA) was used to measure

95 the size distribution of nanoparticles (3–60 nm) every 3 min; the aerosol flow rate was 1.5 L min^{-1} and the sheath flow rate

96 was 15 L min^{-1}. The size distribution data were processed using the method described by Kulmala et al. (2012).

97   Daily ionic species (Na$^+$, Mg^{2+}, K$^+$, NH$_4^+$, NO$_3^-$, SO$_4^{2-}$, and Cl$^-$) in particulate matter and gas data (NH$_3$ and SO$_2$) at

98   Zeppelin Observatory, along with meteorological parameters (temperature, RH, wind, and pressure), were obtained from the

99   Norwegian national monitoring program (Aas et al., 2019) via the EBAS database (http://ebas.nilu.no/). Daily ionic species

100   and gas data are daily measurements collected with a 3-stage filterpack sampler with no size cut-off in the inlet. It should be

101   noted that for the nitrogen compounds the separation of gas and aerosol might be biased due to the volatile nature of NH$_4$NO$_3$.

102   Solar radiation (SRAD) at the AWIPEV observatory in Ny-Alesund were obtained from the Baseline Surface Radiation

103   Network (BSRN) (Maturilli, 2019). Hourly data for number size distributions of particles from 5–810 nm and 10–790 nm,

104   measured with discrete mobility particle sizers (DMPS), were obtained from Stockholm University and the Norwegian Institute

105   for Air Research (NILU), respectively. The data from the DMPS and filterpack measurements are reported to several

106   international monitoring programmes (i.e. EMEP, ACTRIS, GAW-WDCA), and they are openly available from the database

107   infrastructure EBAS.

108   Satellite-derived chlorophyll-α concentration data in the Svalbard region (70–85ºN, 25ºW–50ºE) was obtained from

109   the level-3 product of the Aqua-Moderate Resolution Imaging Spectroradiometer (MODIS) at a 4 km resolution. Air mass

110   backward trajectories arriving at the Zeppelin Observatory were calculated for up to 5 days using the National Oceanic and

111   Atmospheric Administration (NOAA) Hybrid Single Particle Lagrangian Integrated Trajectory (HYSPLIT) model based on

112   Global Data Assimilation System (GDAS) 1° data. A potential source contribution function (PSCF) method (Pekney et al.,

113   2006; Wang et al., 2009; Fleming et al., 2012) was also used to relate the air mass to NPF occurrence by analyzing the residence

114   time of the air mass relative to the concentration of nanoparticles at the receptor site (Wang et al., 2009). In addition, the k-

115   means clustering method, an unsupervised data classification/partitioning approach, was used to classify potential air mass

116   origin along with the size distributions (Beddows et al., 2009; Dall'Osto et al., 2017).

117   The particle GR was calculated as the change rates of representative particle diameters (d$_1$ and d$_2$) with the highest

118   concentrations at particular times (t$_1$ and t$_2$) (Hussein et al., 2005; Kulmala et al., 2012). The CS, which determines how rapidly

119   condensable vapor molecules will condense on the existing aerosols (Kulmala et al., 2012), was calculated from the size

120   distribution data (3–810 nm) with an assumed sulfuric acid diffusion coefficient of 0.117 cm^{-2} s^{-1} (Gong et al., 2010; Cai et al.,

121   2017). The number concentration in the size range d$_i$ to d$_j$ (N$_{i-j}$) was derived from the measured size distribution data.

122   Considering the particle loss and production processes allowed the following balance equation for N$_{i-j}$ to be derived:

123

124
$$\frac{dN_{i-j}}{dt} = J_{i-j} - F_{coag} - F_{growth} \quad (1)$$

125

126   where J$_{i-j}$ is the particle formation rate in the size range of d$_i$ to d$_j$, F$_{coag}$ is the particle loss rate related to coagulation scavenging

127   in the size range of d$_i$ to d$_j$, and F$_{growh}$ is the condensational GR of the nucleation-mode particles. Based on methods suggested

128   by Kulmala et al. (2012), the particle formation rate (J$_{i-j}$) was calculated as:

129

130
$$J_{i-j} = \frac{dN_{i-j}}{dt} + \frac{N_{i-j}}{d_j - d_i} \cdot GR + N_{i-j} CoagS_{i-j} \quad (2)$$

131

132 where $CoagS_{i-j}$ represents the mean of the coagulation sink (CoagS) in the size range of d_i to d_j.

133   The dimensionless criterion (L_Γ), which can be used to predict the occurrence of NPF events (McMurry et al., 2005;

134 Cai et al., 2017), was calculated as:

135

136
$$L_\Gamma = \frac{\bar{c}_1 A_{Fuchs}}{4\beta_{11} N_1 \Gamma} \quad (3)$$

137

138 where $\bar{c}_1$ is the mean thermal velocity of vapor (sulfuric acid), A_{Fuchs} is the Fuchs surface area (a coagulation scavenging

139 parameter), β_{11} is the free molecule collision frequency function for monomer collisions, N_1 is the sulfuric acid number

140 concentration during the nucleation event, and Γ is the growth enhancement factor obtained by dividing the measured GR by

141 the growth determined based on the condensation of only sulfuric acid. The sulfuric acid number concentration was predicted

142 from the measured daily SO_2, hourly CS, hourly solar radiation, and hourly meteorological data (RH and temperature) using

143 the method proposed by Mikkonen et al. (2011).

144

3 Results and discussion

146   The data coverage for the size distribution data collected by nano-SMPS was about 89% during the 27 months

147 sampling period. The monthly variations of the number concentrations of the 3–20 nm nanoparticles (N_{3-20}) and 20–60 nm

148 nanoparticles (N_{20-60}) in 2016–2018 (averaged from hourly data) are shown in Figure 2. Both N_{3-20} and N_{20-60} were highest in

149 summer and lowest in winter, indicating that NPF occurred frequently in summer. The higher SRAD and lower CS (calculated

150 from the 3–810 nm size distribution data) in summer also favored nanoparticle production. The highest monthly SRAD (199

151 W m^{-2}) was observed in June. Due to the higher latitude of the site, the SRAD was lower than values reported at other

152 continental sites (449 W m^{-2} during NPF in Lanzhou, China (Gao et al, 2011); 442–445 W m^{-2} during NPF in Pallas, Finland

153 (Asmi et al., 2011); and 700 W m^{-2} during NPF in Atlanta, USA (Woo et al., 2001)). The wind speed in summer was lower

154 than in other seasons, as expected from local climatology (Maturilli et al., 2013). In addition, marine biogenic sources, which

155 provide gaseous precursors for nanoparticle formation, were abundant in summer. For example, chlorophyll-α concentration

156 (a proxy for marine phytoplankton biomass) in the Arctic Ocean surrounding the observation site from 2016 to 2018 began to

157 increase in April and reached a maximum in May to June (Supplementary Figure S1). During the Arctic haze period, the

158 amount of accumulation-mode particles (>100 nm) increased considerably. A significant CS increase occurred in Mar (Figure

159 2). The high amount of accumulation-mode particles in spring and the high amount of nucleation-mode particles in summer

160 are consistent with previous findings (Tunved et al., 2013; Dall'Osto et al., 2017; Heinzenberg et al., 2017).

161   The size distributions of the 3–60 nm particles from 2016 to 2018 (hourly data) were classified into several major

162 groups using the k-means clustering method. Four distinct clusters were found (Figure 3 (a)), with mode diameters of around

163 10 nm (cluster 1), 20 nm (cluster 2), 30 nm (cluster 3), and 50 nm (cluster 4). Cluster 1 included newly formed particles with

164 high population. Cluster 4 had the lowest ultrafine particles concentration, representing the background condition. The

165 frequencies of each cluster by month are shown in Figure 3 (b). The annual average percentages of each cluster were 7%

166 (cluster 1), 15% (cluster 2), 23% (cluster 3), and 55% (cluster 4). The frequencies of clusters 1 and 2 increased significantly

167 and the cluster 2 was often appeared after the cluster 1 in the late spring and summer months (May, June, July, and August),

168 suggesting that strong particle growth (i.e., increases in mode diameter) after NPF occurred during those months.

169   We identified two distinct types of NPF (Figure 4). In type 1, N_{3-20} increased significantly with subsequent particle

170 growth (the freshly formed particles experienced gradual growth), a typical banana-shaped nucleation event, which is regularly

171 observed at many locations worldwide. In type 2, N_{3-20} increased significantly without clear subsequent particle growth (almost

172 no increase of the mode diameter with time, or not clear for growth); this type of event lasted more than 2 hours. Therefore,

173 the GR could be calculated only for type 1. The cases not matching either of these, they were classified as "undefined" NPF

174 which N_{3-20} increased for a short period of time (less than 2 hours). This NPF classification approach was similar to methods

175 employed previously (Dall Maso et al., 2005; Kulmala et al., 2012; Nguyen et al., 2016). The mean occurrence percentage of

176 NPF days (all types) per year from 2016 to 2018 was ~24%. Dall'Osto et al. (2017) found that the average of yearly NPF

177 occurrence from 2000 to 2010 was 18%, lower than our value, and that this increased over time as the coverage of sea-ice melt

178 increased. In addition, DMS originating from marine sources can be a key precursor contributing to NPF in the remote marine

179 atmosphere. In the Arctic region, the DMS concentration increased by ~33% per decade from 1998 to 2016 (Galí et al., 2019),

180 potentially leading to the increase in the annual NPF occurrence in this area.

181   The highest percentage of NPF occurrence for all types was observed in August (63%) and June (61%), followed by

182 May (47%) and July (44%) as shown in Figure 5. NPF was observed only occasionally in winter during the Arctic night from

183 November to February, consistent with previous observations (Ström et al., 2009; Heintzenberg et al., 2017). Although NPF

184 occurrence could be expected to be lowest in April due to highest CS (Figure 2), that was not the case. Our results showed that

185 NPF occurrence increased significantly in April, was maintained at a high level from May to August, then decreased in

186 September and October. The higher biological and photochemical activity, lower transport of pollutants from mid-latitudes,

187 and increased wet scavenging of particles (low CS) in summer likely favored NPF (Ström et al., 2009). In addition, the melting

188 of sea ice in summer can increase the availability of marine biogenic sources, promoting NPF (Quinn et al., 2008; Tovar-

189 Sánchez et al., 2010; Dall'Osto et al., 2018). Overall, NPF occurrence is mainly affected by the availability of solar radiation

190 (photochemistry) and gaseous precursors in addition to the survivable probability of clusters or particles (Kulmala et al., 2017).

191   A so-called "weak NPF" event, in which initial formation and growth were completed to < 10 nm without further

192 growth, was observed. The weak NPF events documented here could not be detected in previous studies where the minimum

193 detectable size was ~10 nm. The fraction of weak NPF occurrences (out of all NPF occurrences each month) was highest in

194 April (58%) and October (50%), compared to values in May (20%), June (14%), July (7%), August (15%), and September

195 (25%). In April, this was likely caused by the combination of strong solar radiation (i.e., strong photochemistry for production

196 of condensing vapors responsible for particle growth) and high CS; in contrast, October's combination of the low solar

197 radiation (i.e., weak photochemistry) and low CS led to a similar result.

198 NPF lasted for several hours with similar start times (Figure 5). NPF duration was around 6–7 h on average and was

199 longest in summer. Typically, NPF started between 11:00 and 12:00 (UTC), suggesting that photochemical activity with strong

200 solar radiation played an important role in NPF initiation. The variations in start time from month to month (Mar to Nov) were

201 smaller than the monthly variations in NPF occurrence or duration.

202 Figure 6 shows the MODIS monthly chlorophyll-α concentrations around Svalbard, which increased from April and

203 decreased after August, consistent with the NPF occurrence frequency. Full monthly values of satellite-derived chlorophyll-α

204 concentration are summarized in Supplementary Figure S1. The chlorophyll-α concentration was intense in the ocean regions

205 southwest and southeast of Svalbard. A recent study revealed that the DMS production capacity of the Greenland Sea (to the

206 southwest) was 3 times greater than that of the Barents Sea (to the southeast) (Park et al., 2018); this is further discussed in the

207 context of air mass trajectory data in a later section.

208 The existence of significant amounts of nanoparticles as small as 3 nm during NPF events at the study site suggests

209 that NPF occurred there, rather than the particles being transported from other regions after growth. In other words, if NPF

210 occurred at other locations far from the study site, the nanoparticles would have grown during transport to the site and few 3

211 nm particles would have been detected there. To determine the characteristics of particle growth, we calculated the GR in the

212 3–25 nm size range (GR_{3-25}) (Figure 7). The average GR_{3-25} for all months was 2.62 nm h^{-1}, comparable to previously reported

213 GR data (0.2–4.1 nm h^{-1}) in the Arctic region (Kerminen et al., 2018). The highest monthly average GR_{3-25} was observed in

214 July (3.15 nm h^{-1}) and the maximum individual value (7.55 nm h^{-1}) occurred in June. However, the GR_{3-25} was much lower

215 than the values observed in typical urban areas (Table 1), suggesting a lower availability of condensing vapors contributing to

216 particle growth in the Arctic atmosphere. The calculated formation rates of particles down to 3 nm (J_{3-7}) are the first in the

217 Arctic region. The average J_{3-7} during NPF events was 0.1 cm^{-3} s^{-1} in a range from 0.01–1.68 cm^{-3} s^{-1}. The highest monthly

218 average and maximum J_{3-7} were both found in June (0.14 cm^{-3} s^{-1} and 1.68 cm^{-3} s^{-1}, respectively). The formation rate

219 (RSD=55%) varied by month more significantly than for GR_{3-25} (RSD=35%). Values for J_{3-7} (0.01–1.68 cm^{-3} s^{-1}) and J_{3-25}

220 (0.02–1.62 cm^{-3} s^{-1}) were much lower than those reported in continental areas (Stanier et al., 2004; Hamed et al., 2007; Wu et

221 al., 2007; Manninen et al., 2010; Xiao et al., 2015; Shen et al., 2016; Cai et al., 2017). A good linear relationship was found

222 between J_{3-7} and N_{3-7} (r = 0.90; not shown here), indicating that 3–7 nm particles were produced by gas-to-particle conversion

223 rather than direct emissions in the particle phase (i.e., not primary) (Kalivitis et al., 2019). No significant correlation (R^2=0.006,

224 p-value = 0.6) was found between J_{3-7} and GR_{3-25}, suggesting that the vapors participating in the early stage of NPF could be

225 at least partly different from the vapors contributing to subsequent particle growth (Nieminen et al., 2014). However, detailed

226 chemical data for nanoparticles during formation and growth should be obtained to achieve complete understanding of the

227 participating chemical species. Our data indicate that, although NPF occurrence frequency in the Arctic was comparable to

228 continental areas, the J and GR were much lower.

229   Five air mass clusters were found (Figure 8 (a)), representing the contributions of different air masses in different

230 seasons: clusters 1, 2, 3, 4, and 5 represented southwest (slow), south (slow), southeast (fast), northwest (fast), and northeast

231 (fast) air masses, respectively. The air mass speed (travel distance/time) was used to determine whether the air mass was slower

232 or faster compared to the average air mass speed during the measurement period. Cluster 1 dominated in summer, when NPF

233 occurrence was highest; it had the lowest air mass speed, the lowest fraction of land influence (15%), and the highest fraction

234 of time spent over the sea (50%) compared to other air mass clusters. Time spent over sea-ice was 35%. Our data suggest that

235 a slowly moving air mass, which spent most of the time over the ocean and sea-ice is the most favourable for NPF.

236   We further explored the potential source regions of the air masses in relation to NPF using air mass backward

237 trajectory data and the 75th percentile of N_{3-20} (Figure 8 (b)). Increases in the amount of nanoparticles (i.e., NPF events)

238 occurred more frequently when the air mass passed over the oceanic regions to southwest and south of Svalbard (overall, 49%

239 of the air mass during NPF was southwest, i.e., cluster 1). As shown earlier (Figure 6), the chlorophyll-α concentration was

240 strong in the southwest and southeast ocean regions, and the DMS production capacity of the southwest ocean was 3 times

241 greater than that of the southeast ocean (Park et al., 2018). These results suggest that marine biogenic sources from the

242 southwest ocean region play an important role in NPF in the Arctic.

243   We then examined the chemical characteristics of total suspended particles and daily concentration of gaseous NH_3.

244 The seasonal characteristics of ionic species (Na^+, Mg^{2+}, K^+, NH_4^+, NO_3^-, SO_4^{2-}, and Cl^-) in PM from 2016 to 2018

245 (Supplementary Table S1) revealed that the contributions of primary sea salt particles (Na^+, Mg^{2+}, and Cl^-) increased in winter

246 with high wind speeds, while the contributions of NH_4^+, NO_3^-, and SO_4^2 (secondary species) increased in spring and summer.

247 The slope of the cation equivalents (Na^+, Mg^{2+}, K^+, and NH_4^+) versus the anion equivalents (NO_3^-, SO_4^{2-}, and Cl^-) (= 0.98; not

248 shown) suggested that the measured cations were mostly neutralized by the anions (Zhang et al., 2015). These ionic species

249 can exist in large particles, and do not necessarily represent the chemical composition of the nanoparticles, but they can provide

250 information about the overall chemical properties of the particles in different seasons. The concentration of non-sea-salt sulfate

251 (nss-sulfate) was derived from the sulfate and sodium concentrations. The nss-sulfate ratio (nss-sulfate/total sulfate) was

252 significantly higher on NPF event days than on non-event days (p-value < 0.05; Figure 9). The nss-sulfate could have had a

253 secondary origin from the DMS from the sea. The NH_3 could also have been involved in NPF (Kirkby et al., 2011) with strong

254 nucleation rate enhancement (Lehtipalo et al., 2018). Dall'Osto et al. (2017) showed that the NH_3 concentration was higher on

255 NPF event days than on non-event days, similar to the results shown in Figure 9 (p-value < 0.01). NH_3 in the Arctic can

256 originate from biological and animal sources (e.g., seabird colonies) (Tovar-Sánchez et al., 2010; Croft et al., 2016; Dall'Osto

257 et al., 2017) and contribute to NPF.

258   We calculated the NPF criterion (L_Γ) values for NPF event and non-event days (Figure 10). The 20 non-event days

259 when GR could be obtained from pre-existing aerosols were selected for the calculation of the L_Γ (Kuang et al., 2010). The

260 NPF duration time was determined using the proposed method (Kulmala et al., 2012), with the time range of non-event days

set as daytime (06:00–18:00). When NPF occurred, the L_Γ ranged from 0.02–2.39 with a mean and median of 0.47 and 0.37, respectively; most values (95%) were less than 1. The L_Γ values of non-event days ranged from 0.19–14.11 with a mean and a median of 4.27 and 2.09, respectively; most values (90%) were larger than 1. These observations were consistent with previous studies of NPF events in clean or moderately-polluted areas (Tecamac, Atlanta, Boulder, and Hyytiala), ranging from 0.0075–0.66 (Kuang et al., 2010), and in a highly-polluted area (Beijing), ranging from 0.22–1.75 (Cai et al., 2017). Our data suggest that L_Γ can also be useful for determining the occurrence of NPF in the Arctic, but not at 100% certainty. Uncertainties in sulfuric acid concentration inferred from daily SO_2 data (as discussed in the experimental section) and other parameters such as the measured GR and averaging time for L_Γ (i.e., NPF duration time) could contribute to unclear separation of NPF event and non-event days (Figure 10).

4 Conclusions

We examined the characteristics of Arctic NPF at the Mount Zeppelin site by conducting continuous measurements of nanoparticles down to 3 nm size from 2016 to 2018. The size distributions of 3–60 nm particles were classified into distinct clusters with strong seasonal variability and mode diameters of 10 nm (cluster 1), 20 nm (cluster 2), 30 nm (cluster 3), and 50 nm (cluster 4). A significant number of nanoparticles as small as 3 nm often appeared during NPF, particularly in summer, suggesting that there is a good chance that these were produced near the site rather than being transported from other regions after growth. The average NPF occurrence frequency per year was 24%. J_{3-7} averaged 0.1 $cm^{-3} s^{-1}$, ranging from 0.01–1.68 $cm^{-3} s^{-1}$, and GR_{3-25} averaged 2.62 nm h^{-1}, ranging from 0.35–7.55 nm h^{-1}. These data suggest that the NPF occurrence frequency in the Arctic is comparable to those in continental areas although the J and GR were lower in the Arctic. We next identified five major air mass clusters using backward trajectory analysis; PSCF results indicated that air masses from the south and southwest ocean regions were related to the elevated concentrations of nanoparticles at the site. This region was consistent with elevated chlorophyll-α and DMS production capacity, suggesting that marine biogenic sources should play an important role in Arctic NPF. The concentration of gaseous NH_3 was higher on NPF event days than on non-event days, suggesting that marine animal sources also significantly affected Arctic NPF. Previously developed NPF criteria (a low ratio of loss rate to growth rate of clusters favors NPF) were applicable to Arctic NPF occurrence.

Acknowledgements. This research was supported by a National Research Foundation of Korea Grant from the Korean Government (Ministry of Science and ICT) (NRF-2016M1A5A1901779) (KOPRI-PN20081) (Title: Circum Arctic Permafrost Environment Change Monitoring, Future Prediction and Development Techniques of Useful Biomaterials (CAPEC Project)), a National Leading Research Laboratory program (NPF-2019R1A2C3007202) and Samsung Advanced Institute of Technology. The measurements of inorganic components, DMPS (10–790 nm), and meteorological data in air and aerosols at Mount Zeppelin were financed by the Norwegian Environment Agency, while the DMPS (5-810 nm) data were produced by

293 Stockholm University. The meteorological data for solar radiation (SRAD) were provided by the Alfred Wegener Institute
294 (Maturilli, 2019).

295

296 *Data availability.* The nano-SMPS data (3-60 nm) we measured in this publication are available in Korea Polar Data Center
297 (KPDC) web site ('https://kpdc.kopri.re.kr/search/'), and the raw data will be available upon request to the corresponding
298 author (kpark@gist.ac.kr).

299

300 *Competing interests.* The authors declare that they have no conflict of interest.

301

302 **References**

303 Aas, W.; M. Fiebig, S.; Solberg and K. E. Yttri.: Monitoring of long-range transported air pollutants in Norway. Annual report
304   2018, NILU rapport, 2019.

305 Asmi, E.; Kivekäs, N.; Kerminen, V. M.; Komppula, M.; Hyvärinen, A. P.; Hatakka, J.; Viisanen, Y.; Lihavainen, H.:
306   Secondary new particle formation in Northern Finland Pallas site between the years 2000 and 2010, Atmos. Chem. Phys.,
307   11 (24), 12959-12972, https://doi.org/10.5194/acp-11-12959-2011, 2011

308 Asmi, E.; Kondratyev, V.; Brus, D.; Laurila, T.; Lihavainen, H.; Backman, J.; Vakkari, V.; Aurela, M.; Hatakka, J.; Viisanen,
309   Y.; Uttal, T.; Ivakhov, V.; Makshtas, A.: Aerosol size distribution seasonal characteristics measured in Tiksi, Russian
310   Arctic, Atmos. Chem. Phys., 16 (3), 1271-1287, https://doi.org/10.5194/acp-16-1271-2016, 2016.

311 Beddows, D. C.; Dall'Osto, M.; Harrison, R. M.: Cluster analysis of rural, urban, and curbside atmospheric particle size data,
312   Environ. Sci. Technol., 43 (13), 4694-4700, https://doi.org/10.1021/es803121t, 2009.

313 Beine, H.; Argentini, S.; Maurizi, A.; Mastrantonio, G.; Viola, A.: The local wind field at Ny-Ålesund and the Zeppelin
314   mountain at Svalbard, Meteorol. Atmos. Phys., 78 (1-2), 107-113, https://doi.org/10.1007/s007030170009, 2001.

315 Cai, R.; Yang, D.; Fu, Y.; Wang, X.; Li, X.; Ma, Y.; Hao, J.; Zheng, J.; Jiang, J.: Aerosol surface area concentration: A
316   governing factor in new particle formation in Beijing, Atmos. Chem. Phys., 17 (20), 12327-12340,
317   https://doi.org/10.5194/acp-17-12327-2017, 2017.

318 Covert, D. S.; Wiedensohler, A.; Aalto, P.; Heintzenberg, J.; Mcmurry, P. H.; Leck, C.: Aerosol number size distributions
319   from 3 to 500 nm diameter in the arctic marine boundary layer during summer and autumn, Tellus B, 48 (2), 197-212,
320   https://doi.org/10.3402/tellusb.v48i2.15886, 1996.

321 Croft, B.; Martin, R. V.; Leaitch, W. R.; Tunved, P.; Breider, T. J.; D'Andrea, S. D.; Pierce, J. R.: Processes controlling the
322   annual cycle of Arctic aerosol number and size distributions, Atmos. Chem. Phys., 16 (6), 3665-3682,
323   https://doi.org/10.5194/acp-16-3665-2016, 2016.

324 Dal Maso, M.; Kulmala, M.; Riipinen, I.; Wagner, R.; Hussein, T.; Aalto, P. P.; Lehtinen, K. E.: Formation and growth of
325  fresh atmospheric aerosols: eight years of aerosol size distribution data from SMEAR II, Hyytiala, Finland, Boreal
326  Environ. Res., 10 (5), 323-336, 2005.

327 Dall Osto, M.; Beddows, D. C. S.; Tunved, P.; Krejci, R.; Strom, J.; Hansson, H. C.; Yoon, Y. J.; Park, K. T.; Becagli, S.;
328  Udisti, R.; Onasch, T.; CD, O. D.; Simo, R.; Harrison, R. M.: Arctic sea ice melt leads to atmospheric new particle
329  formation, Sci. Rep., 7 (1), 3318, https://doi.org/10.1038/s41598-017-03328-1, 2017.

330 Dall Osto, M.; Geels, C.; Beddows, D. C. S.; Boertmann, D.; Lange, R.; Nojgaard, J. K.; Harrison, R. M.; Simo, R.; Skov, H.;
331  Massling, A.: Regions of open water and melting sea ice drive new particle formation in North East Greenland, Sci. Rep.,
332  8 (1), 6109, https://doi.org/10.1038/s41598-018-24426-8, 2018.

333 Fleming, Z. L.; Monks, P. S.; Manning, A. J.: Untangling the influence of air-mass history in interpreting observed atmospheric
334  composition, Atmos. Res., 104, 1-39, https://doi.org/10.1016/j.atmosres.2011.09.009, 2012.

335 Galí, M.; Devred, E.; Babin, M.; Levasseur, M.: Decadal increase in Arctic dimethylsulfide emission, Proc. Natl. Acad. Sci.
336  U. S. A., 116 (39), 19311-19317, https://doi.org/10.1073/pnas.1904378116, 2019.

337 Gao, J.; Chai, F.; Wang, T.; Wang, W.: Particle number size distribution and new particle formation (NPF) in Lanzhou,
338  Western China, Particuology, 9 (6), 611-618, https://doi.org/10.1016/j.partic.2011.06.008, 2011.

339 Gong, Y.; Hu, M.; Cheng, Y.; Su, H.; Yue, D.; Liu, F.; Wiedensohler, A.; Wang, Z.; Kalesse, H.; Liu, S.; Wu, Z.; Xiao, Z.;
340  Mi, P.; Zhang, Y.: Competition of coagulation sink and source rate: New particle formation in the Pearl River Delta of
341  China, Atmos. Environ., 44, 3278-3285, https://doi.org/10.1016/j.atmosenv.2010.05.049, 2010.

342 Hamed, A.; Joutsensaari, J.; Mikkonen, S.; Sogacheva, L.; Maso, M. D.; Kulmala, M.; Cavalli, F.; Fuzzi, S.; Facchini, M.;
343  Decesari, S.: Nucleation and growth of new particles in Po Valley, Italy, Atmos. Chem. Phys., 7 (2), 355-376,
344  https://doi.org/10.5194/acp-7-355-2007, 2007.

345 Heintzenberg, J.; Leck, C.; Tunved, P.: Potential source regions and processes of the aerosol in the summer Arctic, Atmos.
346  Chem. Phys., 15 (6), 6487-6502, https://doi.org/10.5194/acp-15-6487-2015, 2015.

347 Heintzenberg, J.; Tunved, P.; Galí, M.; Leck, C.: New particle formation in the Svalbard region 2006–2015, Atmos. Chem.
348  Phys., 17 (10), 6153-6175, https://doi.org/10.5194/acp-17-6153-2017, 2017.

349 Hirdman, D.; Burkhart, J. F.; Sodemann, H.; Eckhardt, S.; Jefferson, A.; Quinn, P. K.; Sharma, S.; Ström, J.; Stohl, A.: Long-
350  term trends of black carbon and sulphate aerosol in the Arctic: changes in atmospheric transport and source region
351  emissions, Atmos. Chem. Phys., 10 (19), 9351-9368, https://doi.org/10.5194/acp-10-9351-2010, 2010.

352 Hussein, T.; Dal Maso, M.; Petaja, T.; Koponen, I. K.; Paatero, P.; Aalto, P. P.; Hameri, K.; Kulmala, M.: Evaluation of an
353  automatic algorithm for fitting the particle number size distributions, Boreal Environ. Res., 10 (5), 337-355, 2005.

354 Iziomon, M.; Lohmann, U.; Quinn, P.: Summertime pollution events in the Arctic and potential implications, J. Geophys. Res.:
355  Atmospheres, 111, D12206, https://doi.org/10.1029/2005JD006223, 2006.

356 Järvinen, E.; Virkkula, A.; Nieminen, T.; Aalto, P. P.; Asmi, E.; Lanconelli, C.; Busetto, M.; Lupi, A.; Schioppo, R.; Vitale,
357  V.; Mazzola, M.; Petäjä, T.; Kerminen, V. M.; Kulmala, M.: Seasonal cycle and modal structure of particle number size

358   distribution at Dome C, Antarctica, Atmos. Chem. Phys., 13 (15), 7473-7487, https://doi.org/10.5194/acp-13-7473-2013,
359   2013.

360   Jeffries, M.; Richter-Menge, J.: State of the climate in 2011: The Arctic., Bull. Am. Meteorol. Soc., 93, S127-S148, 2012.

361   Kalivitis, N.; Kerminen, V.-M.; Kouvarakis, G.; Stavroulas, I.; Tzitzikalaki, E.; Kalkavouras, P.; Daskalakis, N.;
362   Myriokefalitakis, S.; Bougiatioti, A.; Manninen, H. E.; Roldin, P.; Petäjä, T.; Boy, M.; Kulmala, M.; Kanakidou, M.;
363   Mihalopoulos, N.: Formation and growth of atmospheric nanoparticles in the eastern Mediterranean: Results from long-
364   term measurements and process simulations, Atmos. Chem. Phys., 19 (4), 2671-2686, https://doi.org/10.5194/acp-19-
365   2671-2019, 2019.

366   Kerminen, V.-M.; Chen, X.; Vakkari, V.; Petäjä, T.; Kulmala, M.; Bianchi, F.: Atmospheric new particle formation and growth:
367   review of field observations, Environ. Res. Lett., 13 (10), https://doi.org/10.1088/1748-9326/aadf3c, 2018.

368   Kim, J.; Yoon, Y. J.; Gim, Y.; Choi, J. H.; Kang, H. J.; Park, K.-T.; Park, J.; Lee, B. Y.: New particle formation events observed
369   at King Sejong Station, Antarctic Peninsula–Part 1: Physical characteristics and contribution to cloud condensation nuclei,
370   Atmos. Chem. Phys., 19 (11), 7583-7594, https://doi.org/10.5194/acp-19-7583-2019, 2019.

371   Kirkby, J.; Curtius, J.; Almeida, J.; Dunne, E.; Duplissy, J.; Ehrhart, S.; Franchin, A.; Gagne, S.; Ickes, L.; Kurten, A.; Kupc,
372   A.; Metzger, A.; Riccobono, F.; Rondo, L.; Schobesberger, S.; Tsagkogeorgas, G.; Wimmer, D.; Amorim, A.; Bianchi,
373   F.; Breitenlechner, M.; David, A.; Dommen, J.; Downard, A.; Ehn, M.; Flagan, R. C.; Haider, S.; Hansel, A.; Hauser, D.;
374   Jud, W.; Junninen, H.; Kreissl, F.; Kvashin, A.; Laaksonen, A.; Lehtipalo, K.; Lima, J.; Lovejoy, E. R.; Makhmutov, V.;
375   Mathot, S.; Mikkila, J.; Minginette, P.; Mogo, S.; Nieminen, T.; Onnela, A.; Pereira, P.; Petaja, T.; Schnitzhofer, R.;
376   Seinfeld, J. H.; Sipila, M.; Stozhkov, Y.; Stratmann, F.; Tome, A.; Vanhanen, J.; Viisanen, Y.; Vrtala, A.; Wagner, P. E.;
377   Walther, H.; Weingartner, E.; Wex, H.; Winkler, P. M.; Carslaw, K. S.; Worsnop, D. R.; Baltensperger, U.; Kulmala, M.:
378   Role of sulphuric acid, ammonia and galactic cosmic rays in atmospheric aerosol nucleation, Nature, 476 (7361), 429-
379   433, https://doi.org/10.1038/nature10343, 2011.

380   Kuang, C.; Chen, M.; Zhao, J.; Smith, J.; McMurry, P. H.; Wang, J.: Size and time-resolved growth rate measurements of 1 to
381   5 nm freshly formed atmospheric nuclei, Atmos. Chem. Phys., 12 (7), 3573-3589, https://doi.org/10.5194/acp-12-3573-
382   2012, 2012.

383   Kuang, C.; Riipinen, I.; Sihto, S. L.; Kulmala, M.; McCormick, A. V.; McMurry, P. H.: An improved criterion for new particle
384   formation in diverse atmospheric environments, Atmos. Chem. Phys., 10 (17), 8469-8480, https://doi.org/10.5194/acp-
385   10-8469-2010, 2010.

386   Kulmala, M.; Kerminen, V. M.; Petaja, T.; Ding, A. J.; Wang, L.: Atmospheric gas-to-particle conversion: why NPF events
387   are observed in megacities?, Faraday Discuss, 200, 271-288, https://doi.org/10.1039/C6FD00257A, 2017.

388   Kulmala, M.; Petaja, T.; Nieminen, T.; Sipila, M.; Manninen, H. E.; Lehtipalo, K.; Dal Maso, M.; Aalto, P. P.; Junninen, H.;
389   Paasonen, P.; Riipinen, I.; Lehtinen, K. E.; Laaksonen, A.; Kerminen, V. M.: Measurement of the nucleation of
390   atmospheric aerosol particles, Nature Protocols, 7 (9), 1651-1667, https://doi.org/10.1038/nprot.2012.091, 2012.

391 Kulmala, M.; Vehkamäki, H.; Petäjä, T.; Dal Maso, M.; Lauri, A.; Kerminen, V. M.; Birmili, W.; McMurry, P. H.: Formation
392   and growth rates of ultrafine atmospheric particles: a review of observations, J. Aerosol Sci., 35 (2), 143-176,
393   https://doi.org/10.1016/j.jaerosci.2003.10.003, 2004.

394 Law, K. S.; Stohl, A.: Arctic air pollution: Origins and impacts, Science, 315 (5818), 1537-1540, https://doi.org/
395   10.1126/science.1137695, 2007.

396 Leaitch, W. R.; Sharma, S.; Huang, L.; Toom-Sauntry, D.; Chivulescu, A.; Macdonald, A. M.; von Salzen, K.; Pierce, J. R.;
397   Bertram, A. K.; Schroder, J. C.: Dimethyl sulfide control of the clean summertime Arctic aerosol and cloud, Elem. Sci.
398   Anth., 1, http://doi.org/10.12952/journal.elementa.000017, 2013.

399 Lehtipalo, K.; Yan, C.; Dada, L.; Bianchi, F.; Xiao, M.; Wagner, R.; Stolzenburg, D.; Ahonen, L. R.; Amorim, A.; Baccarini,
400   A.: Multicomponent new particle formation from sulfuric acid, ammonia, and biogenic vapors, Sci. Adv., 4 (12),
401   eaau5363, http://doi.org/10.1126/sciadv.aau5363, 2018.

402 Manninen, H. E.; Nieminen, T.; Asmi, E.; Gagné, S.; Häkkinen, S.; Lehtipalo, K.; Aalto, P.; Vana, M.; Mirme, A.; Mirme, S.;
403   Hõrrak, U.; Plass-Dülmer, C.; Stange, G.; Kiss, G.; Hoffer, A.; Törő, N.; Moerman, M.; Henzing, B.; de Leeuw, G.;
404   Brinkenberg, M.; Kouvarakis, G. N.; Bougiatioti, A.; Mihalopoulos, N.; amp; apos; Dowd, C.; Ceburnis, D.; Arneth, A.;
405   Svenningsson, B.; Swietlicki, E.; Tarozzi, L.; Decesari, S.; Facchini, M. C.; Birmili, W.; Sonntag, A.; Wiedensohler, A.;
406   Boulon, J.; Sellegri, K.; Laj, P.; Gysel, M.; Bukowiecki, N.; Weingartner, E.; Wehrle, G.; Laaksonen, A.; Hamed, A.;
407   Joutsensaari, J.; Petäjä, T.; Kerminen, V. M.; Kulmala, M.: EUCAARI ion spectrometer measurements at 12 European
408   sites – analysis of new particle formation events, Atmos. Chem. Phys., 10 (16), 7907-7927, https://doi.org/10.5194/acp-
409   10-7907-2010, 2010.

410 Maturilli, M.: Basic and other measurements of radiation and continuous meteorological observations at station Ny-Ålesund
411   (2016-2018), reference list of 72 datasets. Alfred Wegener Institute - Research Unit Potsdam, PANGAEA,
412   doi.pangaea.de/10.1594/PANGAEA.908444, 2019.

413 Maturilli, M.; Herber, A.; König-Langlo, G.: Climatology and time series of surface meteorology in Ny-Ålesund, Svalbard,
414   Earth System Science Data, 5, 155-163, https://doi.org/10.5194/essd-5-155-2013, 2013.

415 McMurry, P. H.; Fink, M.; Sakurai, H.; Stolzenburg, M. R.; Mauldin, R. L.; Smith, J.; Eisele, F.; Moore, K.; Sjostedt, S.;
416   Tanner, D.; Huey, L. G.; Nowak, J. B.; Edgerton, E.; Voisin, D.: A criterion for new particle formation in the sulfur-rich
417   Atlanta atmosphere, J. Geophys. Res, 110, https://doi.org/10.1029/2005JD005901, 2005.

418 Merikanto, J.; Spracklen, D.; Mann, G.; Pickering, S.; Carslaw, K.: Impact of nucleation on global CCN, Atmos. Chem. Phys.,
419   9 (21), 8601-8616, https://doi.org/10.5194/acp-9-8601-2009, 2009.

420 Mikkonen, S.; Romakkaniemi, S.; Smith, J. N.; Korhonen, H.; Petäjä, T.; Plass-Duelmer, C.; Boy, M.; McMurry, P. H.;
421   Lehtinen, K. E. J.; Joutsensaari, J.; Hamed, A.; Mauldin Iii, R. L.; Birmili, W.; Spindler, G.; Arnold, F.; Kulmala, M.;
422   Laaksonen, A.: A statistical proxy for sulphuric acid concentration, Atmos. Chem. Phys., 11 (7), 20141-20179,
423   https://doi.org/10.5194/acp-11-11319-2011, 2011.

424 Neuber, R.; Ström, J.; Hübner, C.; Hermansen, O.; Arya, B. C.; Beichen, Z.; Kallenborn, R.; Karasinki, G.; Ivanov, B.; Moen,
425   J.: Atmospheric research in Ny-Alesund-a flagship programme, Norsk Polarinstitutt, 2011.

426 Nguyen, Q. T.; Glasius, M.; Sørensen, L. L.; Jensen, B.; Skov, H.; Birmili, W.; Wiedensohler, A.; Kristensson, A.; Nøjgaard,
427   J. K.; Massling, A.: Seasonal variation of atmospheric particle number concentrations, new particle formation and
428   atmospheric oxidation capacity at the high Arctic site Villum Research Station, Station Nord, Atmos. Chem. Phys., 16
429   (17), 11319-11336, https://doi.org/10.5194/acp-16-11319-2016, 2016.

430 Nieminen, T.; Asmi, A.; Dal Maso, M.; Aalto, P. P.; Keronen, P.; Petäjä, T.; Kulmala, M.; Kerminen, V.-M.: Trends in
431   atmospheric new-particle formation: 16 years of observations, Boreal Environ. Res., 19, 191-214, 2014.

432 O'Neill, N.; Pancrati, O.; Baibakov, K.; Eloranta, E.; Batchelor, R.; Freemantle, J.; McArthur, L.; Strong, K.; Lindenmaier, R.:
433   Occurrence of weak, sub-micron, tropospheric aerosol events at high Arctic latitudes, Geophys. Res. Lett., 35 (14),
434   L14814, https://doi.org/10.1029/2008GL033733, 2008.

435 Park, K. T.; Lee, K.; Kim, T. W.; Yoon, Y. J.; Jang, E. H.; Jang, S.; Lee, B. Y.; Hermansen, O.: Atmospheric DMS in the
436   Arctic Ocean and its relation to phytoplankton biomass, Glob. Biogeochem. Cycles, 32 (3), 351-359,
437   https://doi.org/10.1002/2017GB005805, 2017.

438 Park, K.-T.; Jang, S.; Lee, K.; Yoon, Y. J.; Kim, M.-S.; Park, K.; Cho, H.-J.; Kang, J.-H.; Udisti, R.; Lee, B.-Y.: Observational
439   evidence for the formation of DMS-derived aerosols during Arctic phytoplankton blooms, Atmos. Chem. Phys., 17 (15),
440   9665-9675, https://doi.org/10.5194/acp-17-9665-2017, 2017.

441 Pekney, N. J.; Davidson, C. I.; Zhou, L.; Hopke, P. K.: Application of PSCF and CPF to PMF-modeled sources of $PM_{2.5}$ in
442   Pittsburgh, Aerosol Sci. Technol., 40 (10), 952-961, https://doi.org/10.1080/02786820500543324, 2007.

443 Quinn, P.; Bates, T.; Baum, E.; Bond, T.; Doubleday, N.; Fiore, A. M.; Flanner, M.; Fridlind, A.; Garrett, T. J.; Koch, D.;
444   Menon, S.; Shindell, D.; Stohl, A.; Warren, S. G.; Short-Lived Pollutants in the Arctic: their climate impact and possible
445   mitigation strategies, Atmos. Chem. Phys., 8, 1723-1735, https://doi.org/10.5194/acp-8-1723-2008, 2008.

446 Quinn, P.; Miller, T.; Bates, T.; Ogren, J.; Andrews, E.; Shaw, G.: A 3-year record of simultaneously measured aerosol
447   chemical and optical properties at Barrow, Alaska, J. Geophys. Res: Atmospheres, 107 (D11), 4130,
448   https://doi.org/10.1029/2001JD001248, 2002.

449 Quinn, P.; Shaw, G.; Andrews, E.; Dutton, E.; Ruoho-Airola, T.; Gong, S.: Arctic haze: current trends and knowledge gaps,
450   Tellus B, 59 (1), 99-114, https://doi.org/10.1111/j.1600-0889.2006.00238.x, 2007.

451 Radke, L. F.; Lyons, J. H.; Hegg, D. A.; Hobbs, P. V.; Bailey, I. H.: Airborne observations of Arctic aerosols. I: Characteristics
452   of Arctic haze, Geophys. Res. Lett, 11 (5), 393-396, https://doi.org/10.1029/GL011i005p00393, 1984.

453 Satheesh, S.; Moorthy, K. K.: Radiative effects of natural aerosols: A review, Atmos. Environ., 39 (11), 2089-2110,
454   https://doi.org/10.1016/j.atmosenv.2004.12.029, 2005.

455 Sharma, S.; Ishizawa, M.; Chan, D.; Lavoué, D.; Andrews, E.; Eleftheriadis, K.; Maksyutov, S.: 16-year simulation of Arctic
456   black carbon: Transport, source contribution, and sensitivity analysis on deposition, J. Geophys. Res.: Atmospheres, 118
457   (2), 943-964, https://doi.org/10.1029/2012JD017774, 2013.

458 Shaw, G. E.: The Arctic haze phenomenon, Bull. Amer. Meteorol. Soc., 76 (12), 2403-2414, https://doi.org/10.1175/1520-
459   0477(1995)076<2403:TAHP>2.0.CO;2, 1995.

460 Shen, L.; Wang, H.; Lu, S.; Li, L.; Yuan, J.; Zhang, X.; Tian, X.; Tang, Q.: Observation of aerosol size distribution and new
461   particle formation at a coastal city in the Yangtze River Delta, China, Sci. Total Environ., 565, 1175-1184,
462   https://doi.org/10.1016/j.scitotenv.2016.05.164, 2016.

463 Shen, X.; Sun, J.; Zhang, X.; Zhang, Y.; Zhang, L.; Fan, R.: Key features of new particle formation events at background sites
464   in China and their influence on cloud condensation nuclei, Front. Environ. Sci Eng., 10 (5),
465   https://doi.org/10.1007/s11783-016-0833-2, 2016.

466 Stanier, C. O.; Khlystov, A. Y.; Pandis, S. N.: Nucleation Events During the Pittsburgh Air Quality Study: Description and
467   Relation to Key Meteorological, Gas Phase, and Aerosol Parameters, Aerosol Sci. Technol., 38 (sup1), 253-264,
468   https://doi.org/10.1080/02786820390229570, 2004.

469 Ström, J.; Engvall, A.-C.; Delbart, F.; Krejci, R.; Treffeisen, R.: On small particles in the Arctic summer boundary layer:
470   observations at two different heights near Ny-Ålesund, Svalbard, Tellus B, 61 (2), 473-482,
471   https://doi.org/10.3402/tellusb.v61i2.16845, 2009.

472 Ström, J.; Umegård, J.; Tørseth, K.; Tunved, P.; Hansson, H. C.; Holmén, K.; Wismann, V.; Herber, A.; König-Langlo, G.:
473   One year of particle size distribution and aerosol chemical composition measurements at the Zeppelin Station, Svalbard,
474   March 2000–March 2001, Phys. Chem. Earth, Parts A/B/C 2003, 28 (28-32), 1181-1190,
475   https://doi.org/10.1016/j.pce.2003.08.058, 2003.

476 IPCC, 2014: Climate Change 2014: Synthesis Report. Contribution of Working Groups I, II and III to the Fifth Assessment
477   Report of the Intergovernmental Panel on Climate Change [Core Writing Team, R.K. Pachauri and L.A. Meyer (eds.)].
478   IPCC, Geneva, Switzerland, 151 pp.

479 Toon, O. B.; Pollack, J. B.: Atmospheric aerosols and climate: Small particles in the Earth's atmosphere interact with visible
480   and infrared light, altering the radiation balance and the climate, American Scientist, 68 (3), 268-278,
481   https://www.jstor.org/stable/27849822, 1980.

482 Tovar-Sánchez, A.; Duarte, C. M.; Alonso, J. C.; Lacorte, S.; Tauler, R.; Galbán-Malagón, C.: Impacts of metals and nutrients
483   released from melting multiyear Arctic sea ice, J. Geophys. Res., 115 (C7), https://doi.org/10.1029/2009JC005685, 2010.

484 Tunved, P.; Ström, J.; Krejci, R.: Arctic aerosol life cycle: linking aerosol size distributions observed between 2000 and 2010
485   with air mass transport and precipitation at Zeppelin station, Ny-Ålesund, Svalbard, Atmos. Chem. Phys., 13 (7), 3643-
486   3660, https://doi.org/10.5194/acp-13-3643-2013, 2013.

487 Venzac, H.; Sellegri, K.; Laj, P.; Villani, P.; Bonasoni, P.; Marinoni, A.; Cristofanelli, P.; Calzolari, F.; Fuzzi, S.; Decesari, S.:
488   High frequency new particle formation in the Himalayas, Proc. Natl. Acad. Sci., 105 (41), 15666-15671,
489   https://doi.org/10.1073/pnas.0801355105, 2008.

490 Wang, Y.; Zhang, X.; Draxler, R. R.: TrajStat: GIS-based software that uses various trajectory statistical analysis methods to
491   identify potential sources from long-term air pollution measurement data, Environ. Modelling Softw., 24 (8), 938-939,
492   https://doi.org/10.1016/j.envsoft.2009.01.004, 2009.

493 Wang, Z.; Wu, Z.; Yue, D.; Shang, D.; Guo, S.; Sun, J.; Ding, A.; Wang, L.; Jiang, J.; Guo, H.; Gao, J.; Cheung, H. C.;
494   Morawska, L.; Keywood, M.; Hu, M.: New particle formation in China: Current knowledge and further directions, Sci.
495   Total Environ., 577, 258-266, https://doi.org/10.1016/j.scitotenv.2016.10.177, 2017.

496 Weller, R.; Schmidt, K.; Teinilä, K.; Hillamo, R.: Natural new particle formation at the coastal Antarctic site Neumayer, Atmos.
497   Chem. Phys., 15 (19), 11399-11410, https://doi.org/10.5194/acp-15-11399-2015, 2015.

498 Wiedensohler, A.; Covert, D. S.; Swietlicki, E.; Aalto, P.; Heintzenberg, J.; Leck, C.: Occurrence of an ultrafine particle mode
499   less than 20 nm in diameter in the marine boundary layer during Arctic summer and autumn, Tellus B, 48 (2), 213-222,
500   https://doi.org/10.3402/tellusb.v48i2.15887, 1996.

501 Willis, M. D.; Burkart, J.; Thomas, J. L.; Köllner, F.; Schneider, J.; Bozem, H.; Hoor, P. M.; Aliabadi, A. A.; Schulz, H.;
502   Herber, A. B.: Growth of nucleation mode particles in the summertime Arctic: a case study, Atmos. Chem. Phys., 16 (12),
503   7663-7679, https://doi.org/10.5194/acp-16-7663-2016, 2016.

504 Woo, K. S.; Chen, D. R.; Pui, D. Y. H.; McMurry, P. H.: Measurement of Atlanta Aerosol Size Distributions: Observations of
505   Ultrafine Particle Events, Aerosol Sci. Technol., 34 (1), 75-87, https://doi.org/10.1080/02786820120056, 2010.

506 Wu, Z.; Hu, M.; Liu, S.; Wehner, B.; Bauer, S.; Ma ßling, A.; Wiedensohler, A.; Petäjä, T.; Dal Maso, M.; Kulmala, M.: New
507   particle formation in Beijing, China: Statistical analysis of a 1-year data set, J. Geophys. Res., 112 (D9),
508   https://doi.org/10.1029/2006JD007406, 2007.

509 Xiao, S.; Wang, M. Y.; Yao, L.; Kulmala, M.; Zhou, B.; Yang, X.; Chen, J. M.; Wang, D. F.; Fu, Q. Y.; Worsnop, D. R.;
510   Wang, L.: Strong atmospheric new particle formation in winter in urban Shanghai, China, Atmos. Chem. Phys., 15 (4),
511   1769-1781, https://doi.org/10.5194/acp-15-1769-2015, 2015.

512 Yu, H.; Ren, L.; Kanawade, V. P.: New particle formation and growth mechanisms in highly polluted environments, Curr.
513   Pollut. Rep., 3 (4), 245-253, https://doi.org/10.1007/s40726-017-0067-3, 2017.

514 Zhang Y.; Zhang H.-H.; Yang G.-P.; Liu Q.-L.: Chemical Characteristics and Source Analysis of Aerosol Composition over
515   the Bohai Sea and the Yellow Sea in Spring and Autumn, J. Atmos. Sci., 72 (9), 3563-3573, https://doi.org/10.1175/JAS-
516   D-14-0372.1, 2015.

517
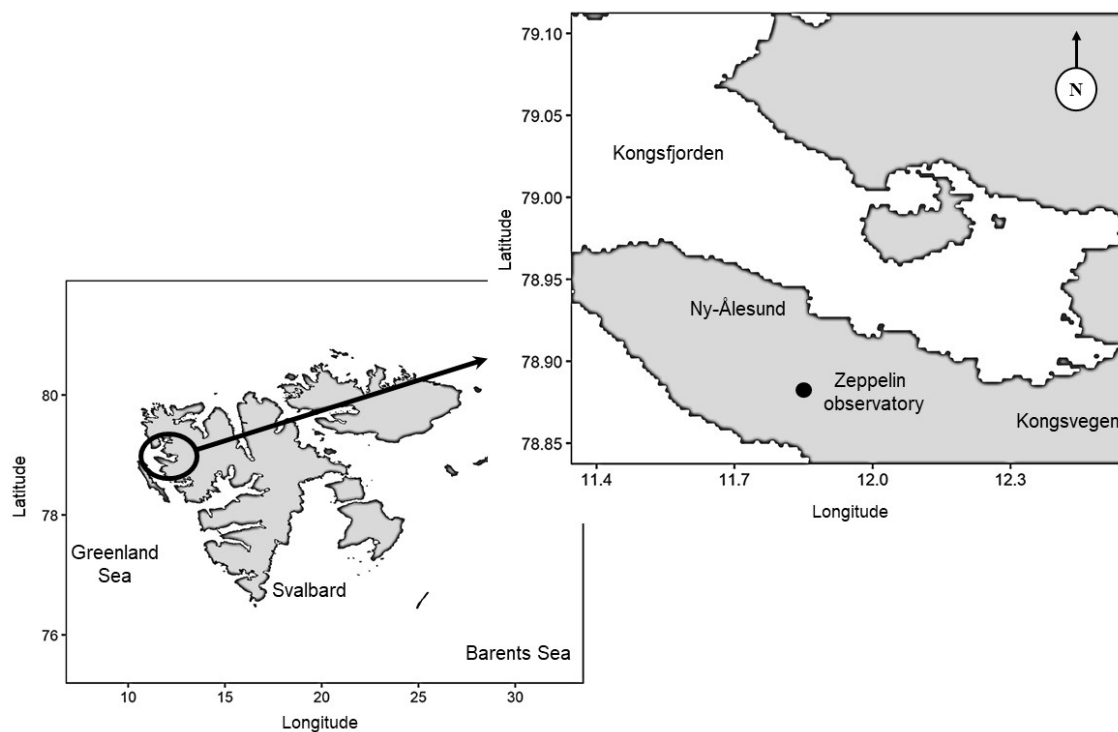
518

519   Figure 1. Measurement site (Zeppelin Observatory) in the Svalbard Archipelago, Ny-Ålesund, Norway.

520
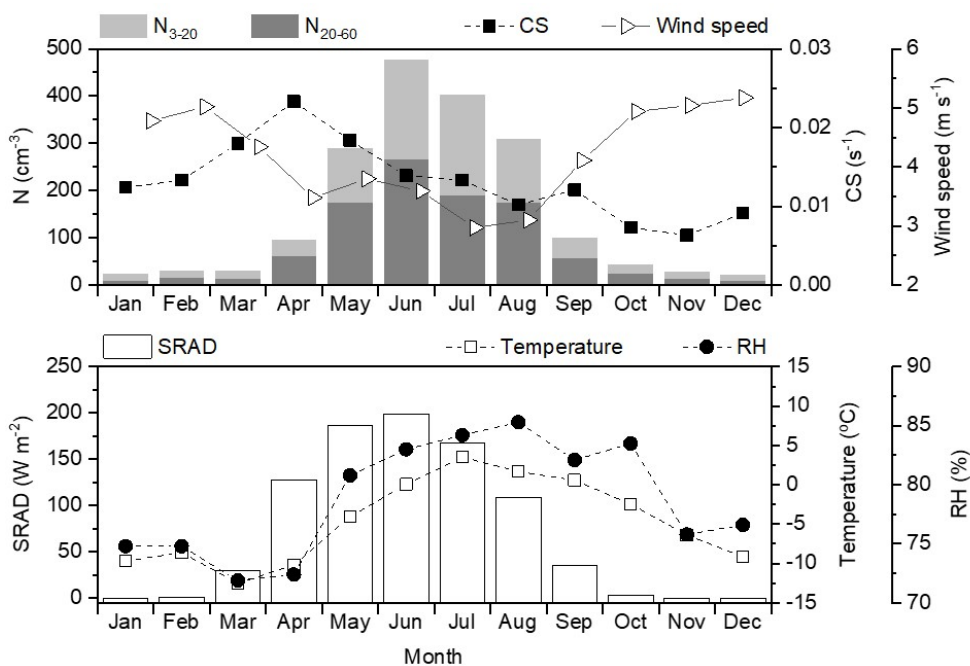
521

522   Figure 2. Monthly variations of N_{3-20}, N_{20-60}, CS, and wind speed (upper panel), temperature, RH, and SRAD [37] (lower panel)

523   from 2016 to 2018.

524

(a)

(b)
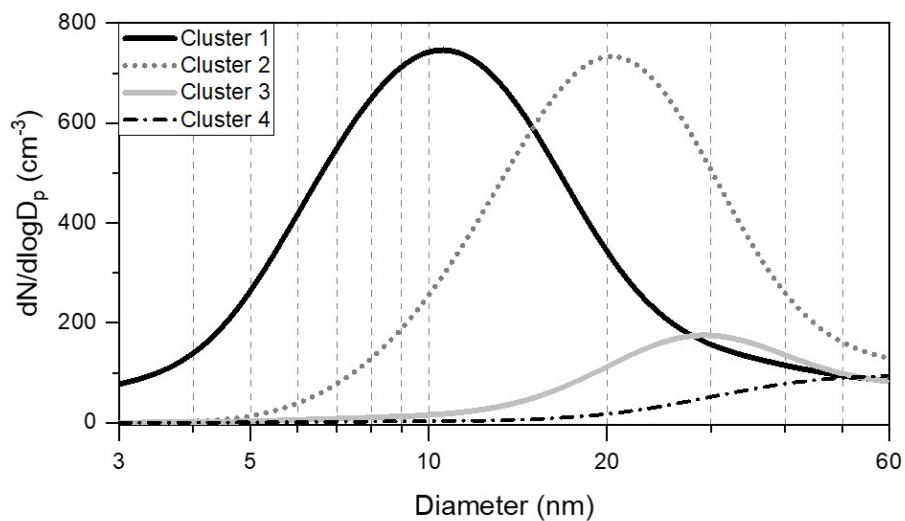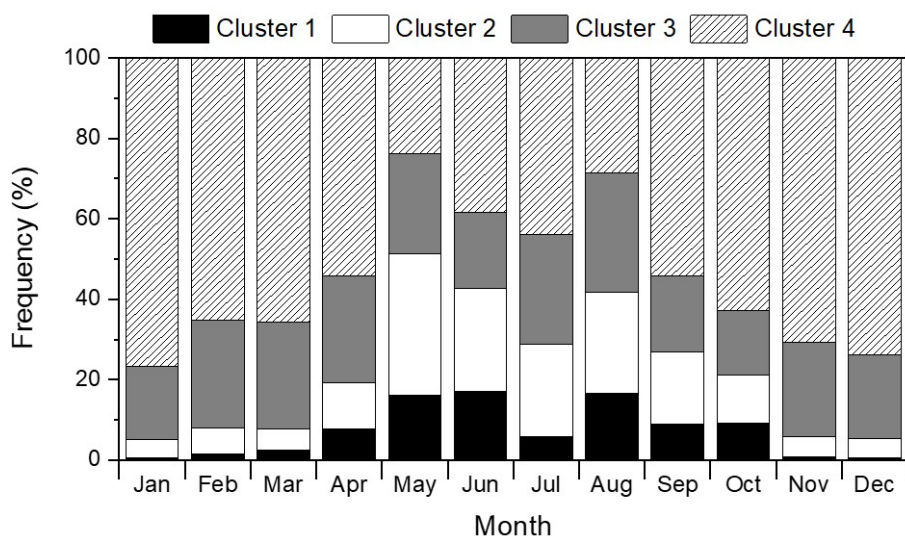
Figure 3. Major particle clusters by (a) size distribution and (b) monthly frequency from 2016 to 2018.

531
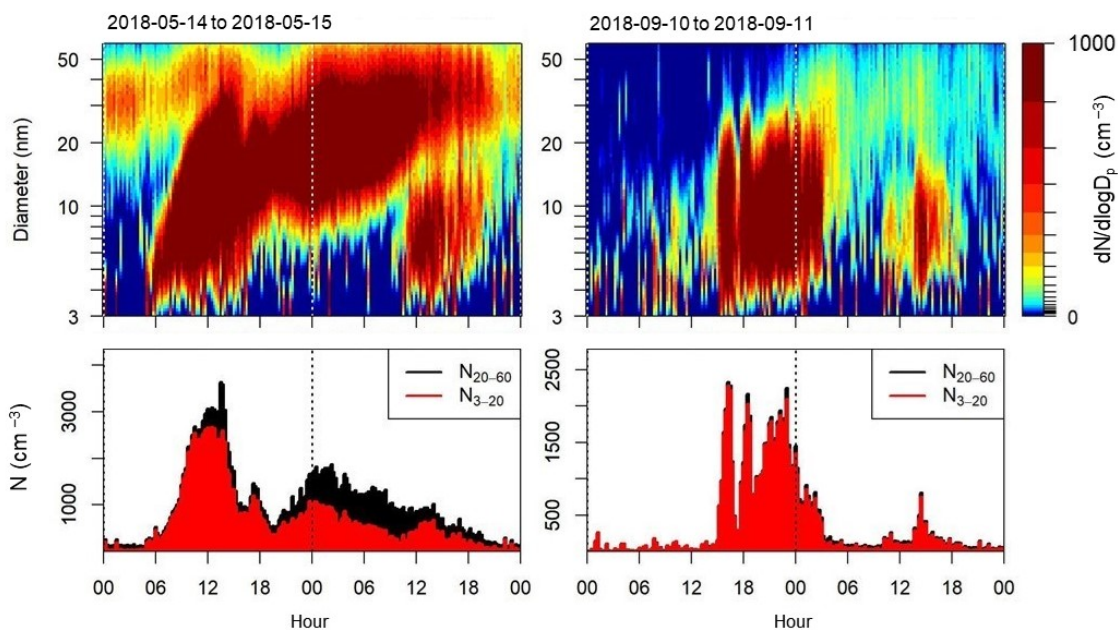
Figure 4. Examples of distinct NPF types identified in this study. In type 1 (left), N_{3-20} increases significantly with continuous

particle growth, while in type 2 (right) it increases significantly without significant particle growth.

534
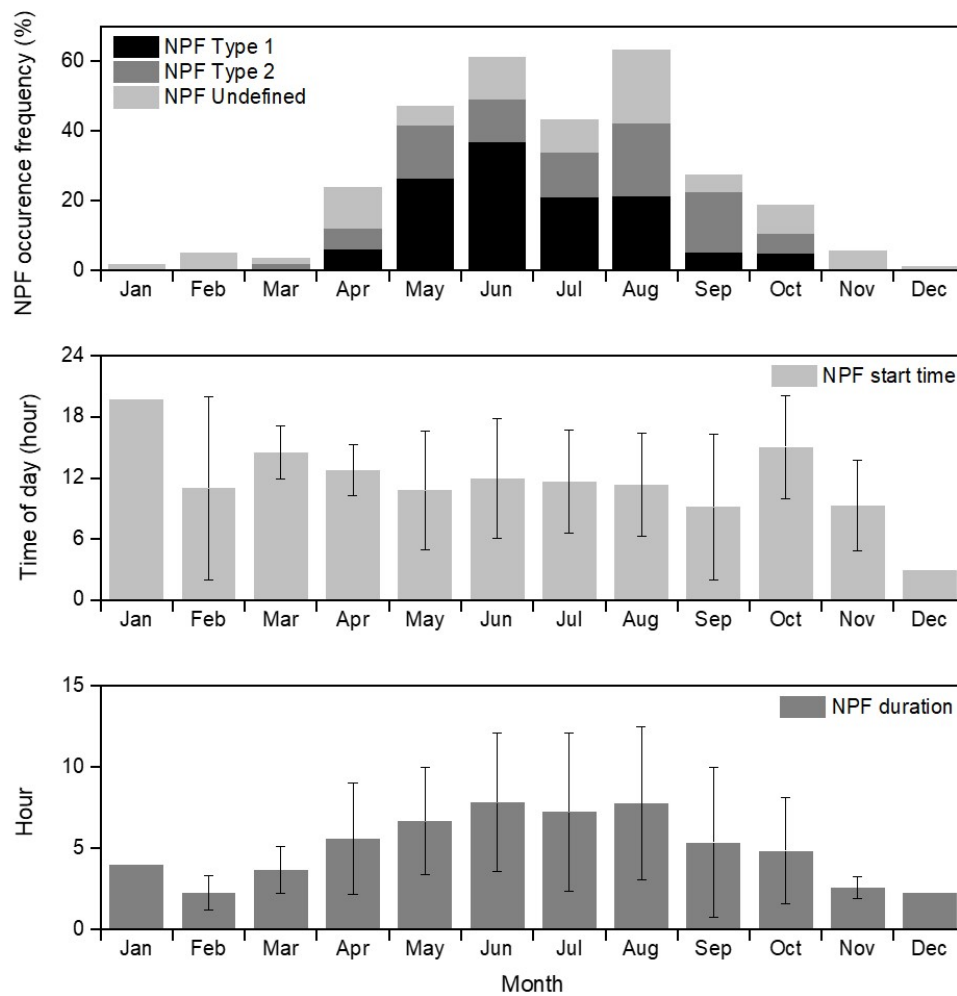
535

536   Figure 5. Monthly variations of NPF occurrence, start time (UTC), and duration; error bar represents standard deviation.

537

538
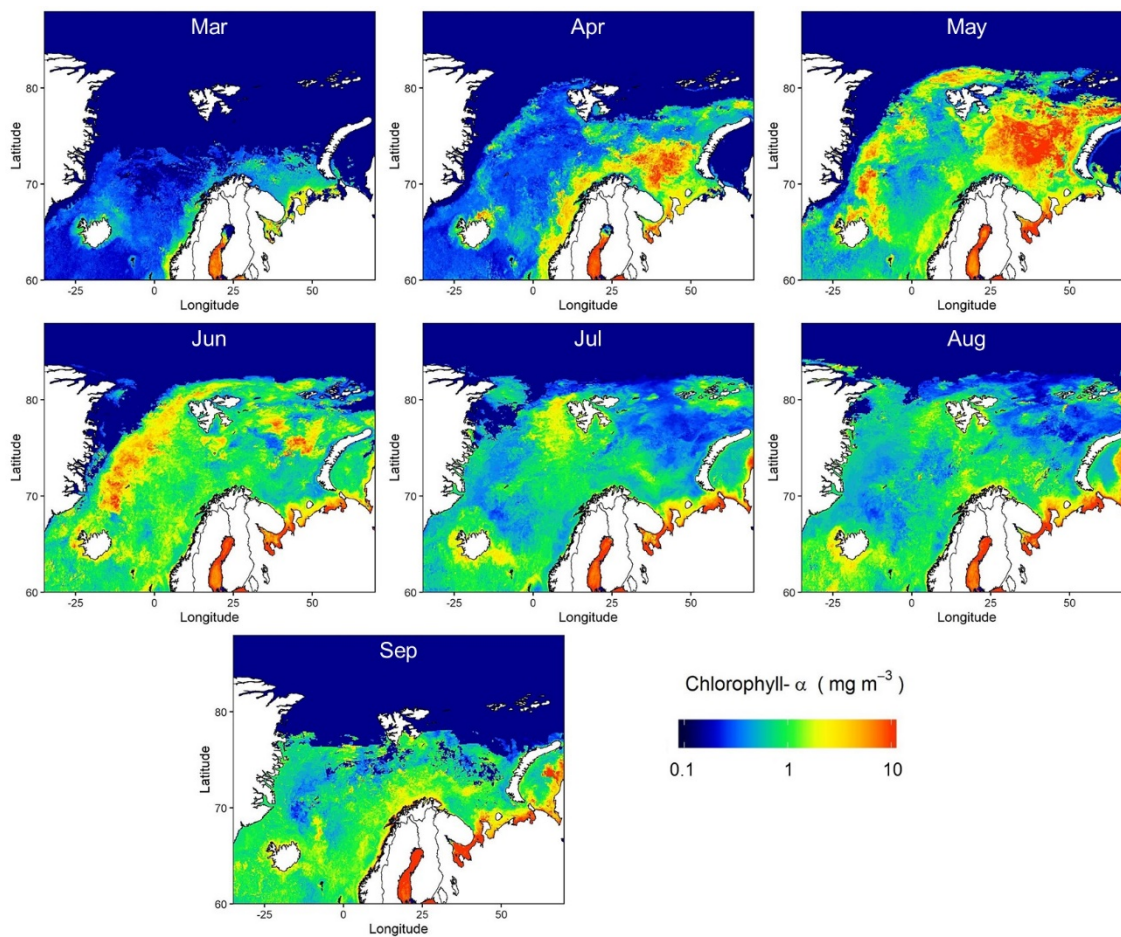
Figure 6. MODIS-derived monthly chlorophyll-α concentration from 2016 to 2018 at 4 km resolution.

540

541

542
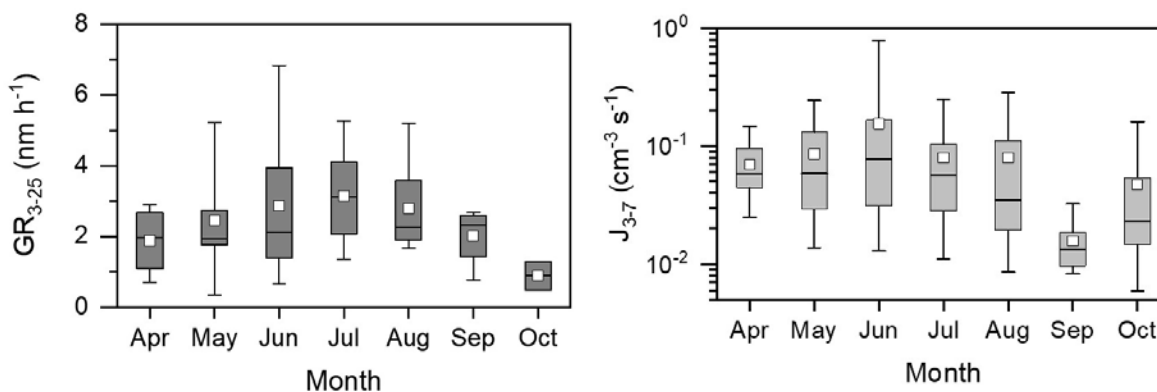
Figure 7. Monthly variations of GR_{3-25} and J_{3-7} for NPF in the Arctic. Boxes and whiskers represent the 25th–75th percentiles

and 10th–90th percentiles, respectively; squares indicate means and horizontal lines within boxes indicate medians.

545

546

547

548

(a)

549

550

(b)
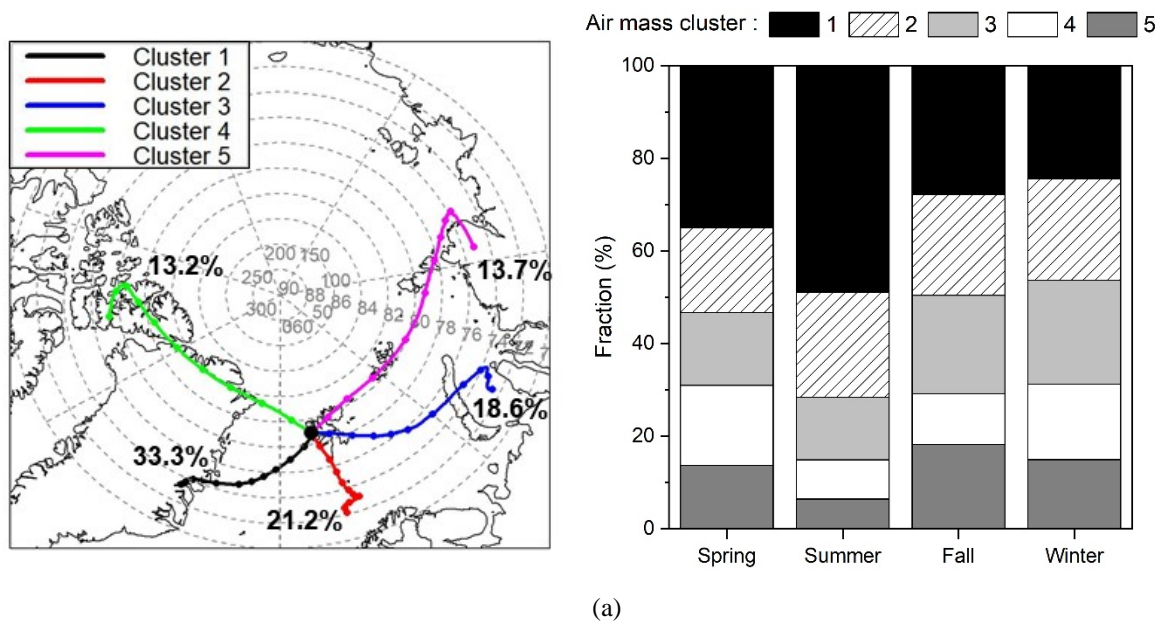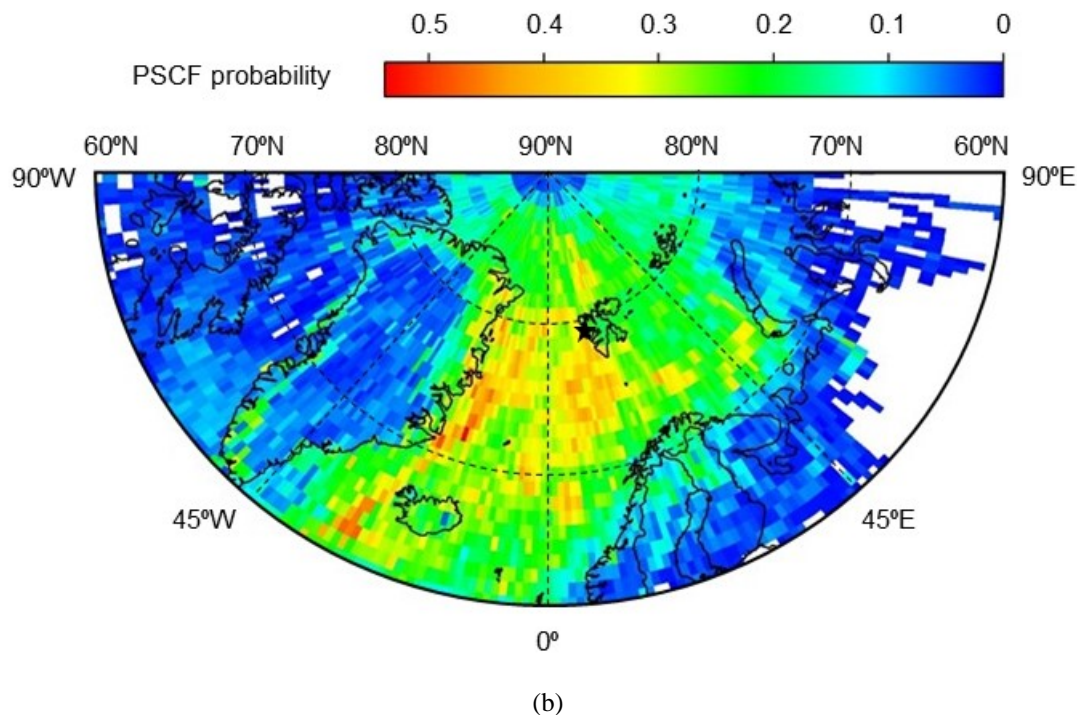
551 Figure 8. (a) Five major clusters for air mass back trajectories from 2016 to 2018 and the fraction of each cluster by seasons.

552 (b) PSCF back-trajectory analysis for air mass origins affecting NPF at the 75th percentile of N_{3-20}.

553
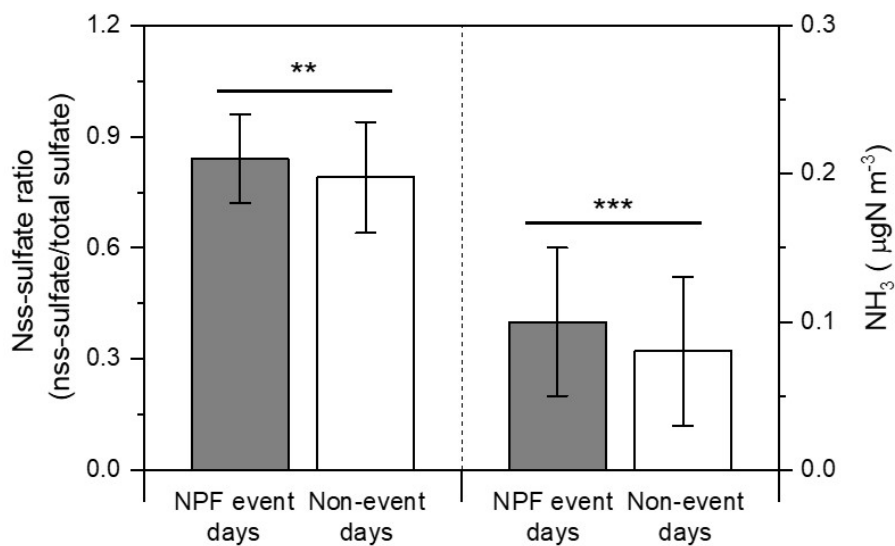
554

555 Figure 9. Comparison of average nss-sulfate ratio (nss-sulfate/total sulfate) and concentration of NH_3 between NPF events and

556 non-event days: error bar and stars represent the standard deviation and *p*-values of a t-test (**: < 0.05 and ***: < 0.01),

557 respectively.

558

10.5194/acp-2020-390
2020-05-08
Author(s) 2020. CC BY 4.0 License.

559
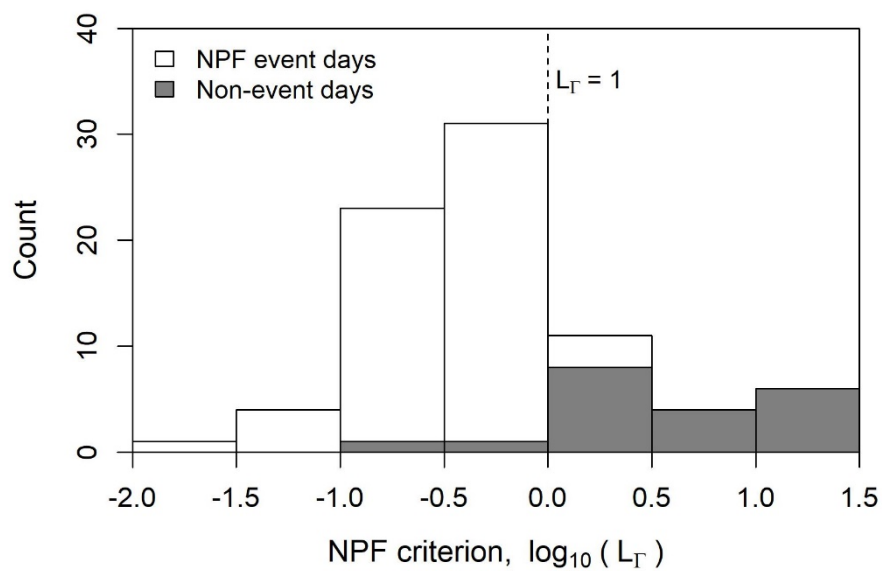
560

561 Figure 10. Distribution of NPF criterion (L_Γ) values for NPF event days (white) and non-event days (grey) in the Arctic.

562

Table 1. Summary of NPF frequency, J, and GR at various sampling sites, including the present study.

Site name and characteristics		Period	NPF frequency	GR (nm h⁻¹)		J (cm⁻³ s⁻¹)		Reference
Zeppelin, Norway	Arctic	2016 to 2018	24%	GR_{3-25}	0.35–7.55	J_{3-7} J_{3-25}	0.01–1.68 0.02–1.62	This study
Finokalia, Greece	Marine background	Jun 2008 to Jun 2018	27%	GR_{9-25}	5.4±3.9	J_{9-25}	0.9±1.2	Kalivitis et al. (2019)
Beijing, China	Urban	Mar 2004 to Feb 2005	40%	GR_{3-25}	0.1–11.2	J_{3-25}	3.3–81.4	Wu et al. (2007)
Pittsburgh, USA	Urban	Jul 2001 to Jun 2002	30%	N/A	N/A	N/A	N/A	Stanier et al. (2004)
San Pietro Capofiume, Italy	Sub-urban	Mar 2002 to Mar 2005	36%	GR_{3-20}	2.9–22.9	J_{3-20}	0.2–36.9	Hamed et al. (2007)
12 European sites (EUCAARI project)[a]	Rural and background	2008 to 2009	21–57%	GR_{7-20}	3.6–6.8	J_{2-3}	0.7–32.4	Manninen et al. (2010)
Hyytiala, Finland	Rural	1996 to 2003	>24%	GR_{3-25}	0.9–5.3	J_{3-25}	0.2–1.1	Dal Maso et al. (2005)
ShangDianzi station, China	Rural	Mar 2008 to Dec 2013	36%	GR_{3-25}	0.7–13.4	J_{3-25}	0.5–39.3	Shen et al. (2016)
Pyramid, Nepal	Himalayas	Mar 2006 to Aug 2007	>35%	GR_{10-20}	1.8 ± 0.7	J_{10-20}	0.05–0.2	Venzac et al. (2008)
Dome C	Antarctica	Dec 2007 to Nov 2009	5–54%	GR_{10-25}	0.5–4.6	J_{10-25}	0.022–0.11	Jarvinen et al. (2013)
Neumayer	Antarctica	Jan 2012 to Mar 2012 Feb 2014 to Apr 2014	N/A	GR_{3-25}	0.4–1.9	J_{3-25}	0.02–0.1	Weller et al. (2015)

| King Sejong | Antarctica | Mar 2009 to Dec 2016 | 6% | $GR_{10\text{-}25}$ | 0.02–3.09 | $J_{2.5\text{-}10}$ | 0.16-9.88 | Kim et al. (2019) |
| Nord, Greenland | Arctic | Jul 2010 to Feb 2013 | 17–38% | N/A | N/A | N/A | N/A | Nguyen et al. (2016) |

[a] Pallas and Hyytiala (Finland), Vavihill (Sweden), Mace Head (Ireland), Cavauw (Netherlands), Melpitz and
565 Hohenpeissenberg (Germany), K-Puszta (Hungary), Jungfraujoch (Switzerland), Puy de Dome (France), San Pietro
Capofiume (Italy), and Finokalia (Greece).